Available online at www.sciencedirect.com

SciVerse ScienceDirect

Ceramics International 39 (2013) 7577–7581

CERAMICS INTERNATIONAL

www.elsevier.com/locate/ceramint

Effect of annealing process on the growth and surface properties of Au–ZnO nanowire films grown by chemical routes

Farid Jamali-Sheini[a,*], Ramin Yousefi[b], M.R. Mahmoudian[c]

[a]Department of Physics, Ahwaz Branch, Islamic Azad University, Ahwaz, Iran
[b]Department of Physics, Masjed-Soleiman Branch, Islamic Azad University (I.A.U.), Masjed-Soleiman, Iran
[c]Department of Chemistry, Shahid Sherafat, University of Farhangian, Tehran 15916, Iran

Received 21 December 2012; received in revised form 4 March 2013; accepted 4 March 2013
Available online 13 March 2013

Abstract

Au–ZnO nanowire films have been synthesized by chemical routes, electrochemical deposition (ECD) and chemical bath deposition (CBD) techniques, on zinc foil followed by annealing in air at 400 °C. X-ray diffraction patterns reveal formation of the ZnO wurtzite structure along with binary phases Au_3Zn and $AuZn_3$. Scanning electron microscopy shows the presence of ZnO nanowires having several micrometers in length and less than 120 nm in diameter synthesized by ECD and in the range of 70–400 nm using the CBD technique. During the annealing process, different surface morphologies originating from different catalytic effects of Au atoms/layers were observed. In addition, the effect of synthesis routes on crystalline quality and optical properties were studied by Raman and photoluminescence spectrometers indicating varying concentration of defects on the films. The Raman results indicate that Au–ZnO nanowire film prepared by chemical bath deposition route had better crystalline quality.

Keywords: D. ZnO; Nanowires; Electrochemical deposition; Chemical bath deposition; Photoluminescence

1. Introduction

Semiconductors in the form of thin films and/or nanostructured films have received extensive attention due to unique physical and chemical properties with numerous potential applications specifically different from bulk semiconductors. Among various semiconductors, zinc oxide (ZnO), having a wide band-gap (3.37 eV) and large excitation binding energy (60 meV), is a versatile smart material that has technological application in catalysis, sensors, piezoelectric, surface acoustic, light emitting and field emission devices [1]. So far, well-defined ZnO nanostructures with a variety of morphology such as rods, wires, needles, funnels, tubes, disks, donuts, bridges, nails and hierarchicals have been achieved through vapor-phase and solution-phase methods [2–8]. The vapor-phase method requires an expensive equipment to generate extreme conditions such as high temperature and/or low pressure compared with the solution-phase method.

In order to have desirable electrical, optical and other properties of ZnO nanostructures/films, it is practical to dope/decorate ZnO with other elements by different methods. In addition to many reports on the synthesis and characterization of metal-ZnO nanostructures, noble metals such as Au (Ag, Pt and Pd)–ZnO, are of considerable interested due to their novel and/or remarkable performances [9–13]. For instance in our previous works, Au–ZnO nanowire arrays were synthesized using a vacuum evaporation system and thermal oxidation process. The results showed an enhancement in the field emission properties and also a highly hydrophilic surface was obtained [12,13]. Because of the presence of Au atoms in the ZnO nanostructures, as compared with the undoped ZnO, a different optical property was also observed. It is believed that doping/decorating ZnO with a noble metal may lead to novel or enhanced performance. Moreover, a little work has so far been performed on surface properties of nanostructures modified by these metals. Therefore in this

*Corresponding author. Tel.: +98 916 111 4457.
E-mail addresses: faridjamali@iau.ahvaz.ac.ir, faridjamali2003@yahoo.com (F. Jamali-Sheini).

0272-8842/$ - see front matter © 2013 Elsevier Ltd and Techna Group S.r.l. All rights reserved.
http://dx.doi.org/10.1016/j.ceramint.2013.03.011

experiment, a combination of two techniques such as chemical routes (electrochemical deposition and chemical bath deposition techniques) and annealing processes have been chosen for synthesizing Au–ZnO nanowire films.

The main objective of the present work is to study the influence of different chemical routes on the growth process and surface properties of Au–ZnO nanowire films. Optical characterization of the products reveals different defects from each synthesis route.

2. Experimental details

2.1. Synthesis

The ZnO nanostructures were prepared by annealing (thermal oxidation) zinc foil coated with a thin layer of gold. The deposition of gold layers was carried out by two techniques. The first was an electrochemical deposition (ECD) technique, using a mixture of $ZnCl_2$, H_2O_2 and $HAuCl_4 \cdot 3H_2O$ (analytical grade) in concentrations of ~0.016 M, ~0.04 M and ~0.001 M, respectively. The volume ratio of $ZnCl_2 - H_2O_2$ and $HAuCl_4 \cdot 3H_2O$ was set at 9:1. The experiments were performed in a conventional three-electrode electrochemical cell, in which a polycrystalline Zn foil (size: 1 cm × 2 cm and purity: ~99.99%, Alfa Aesar), a Pt sheet (1 cm × 2 cm) and a saturated calomel electrode (SCE) served as the working, counter, and reference electrodes, respectively. A computer controlled electrochemical analyzer (Model-1100A Series, CH Instrument, USA) was used to maintain the cathodic polarization condition at −1.2 V with respect to the SCE. The electrolyte was constantly stirred during the synthesis. After a fixed deposition time of 20 min the working electrode was removed from the electrolyte, washed in a gentle flow of distilled water, and dried in air. A second experiment was carried out using a chemical bath deposition (CBD) technique immersing the substrates in an aqueous solution containing 0.001 M of $HAuCl_4 \cdot 3H_2O$ (analytical grade). Before the deposition experiments the solutions were stirred for 5 min after which Zn foil was dipped into the solution for 20 s, rinsed with distilled water and dried in air. The solution was maintained at 80 ± 2 °C and prior to each experiment, the Zn foil and Pt sheet were mechanically polished and ultrasonically cleaned in acetone and methanol, for 15 min in each. After deposition, the substrates were placed in a laboratory furnace and annealed in air at 400 °C for 4 h. The films prepared using the ECD and CBD techniques are named specimens A and B, respectively.

At least three specimens were synthesized under identical experimental conditions via each route and characterized by various analytical techniques in order to check reproducibility and repeatability of the results.

2.2. Characterization

The crystal structure of the films was studied using an X-ray diffractometer (XRD) equipped with a monochromatized Cukα radiation source (λ=1.54178 Å) using a D8, Advance, Bruker AXS. The surface morphology and composition of the ZnO films were characterized by scanning electron microscopy (SEM) and energy dispersive X-ray spectroscopy (EDS) using a JEOL, JSM-6360A. Optical properties were derived from photoluminescence (PL) spectra recorded at room temperature. The PL was measured with a Perkin-Elmer-LS-55, photoluminescence spectrometer using a Xenon lamp as the source with excitation wavelength ~305 nm. Raman spectra were measured with a Jobin Yvon Horiba HR 800UV Raman spectrometer using an Ar ion laser with excitation wavelength ~514.5 nm over the wavelength range 350–650 nm.

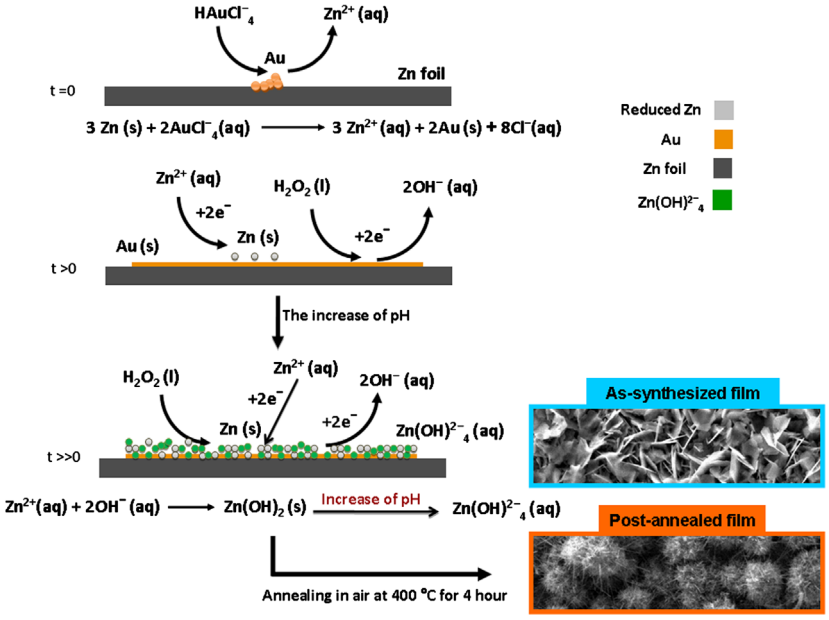

Fig. 1. Schematic illustration of Au–ZnO growth process.

3. Results and discussion

When the zinc foil was immersed in the solution, a thin layer of gold was deposited on the zinc substrate. The following reaction between the zinc and $HAuCl_4^-$ occurred on the zinc surface of both specimens (A and B) at the earlier growth stage.

$$Zn(s) \rightarrow Zn^{2+}(aq) + 2e^- \quad (1)$$

$$AuCl_4^-(aq) + 3e^- \rightarrow Au(s) + 4Cl^-(aq) \quad (2)$$

$$3Zn(s) + 2AuCl_4^-(aq) \rightarrow 3Zn^{2+}(aq) + 2Au(s) + 8Cl^-(aq) \quad (3)$$

In case of specimen A, H_2O_2 in the solution reacted with the zinc foil, which is not covered with gold.

$$Zn(s) \rightarrow Zn^{2+}(aq) + 2e^- \quad (4)$$

$$H_2O_2(1) + 2e^- \rightarrow 2OH^-(aq) \quad (5)$$

$$Zn(s) + H_2O_2(1) \rightarrow Zn(OH)_2(s) \quad (6)$$

When a voltage was applied, the concentration of OH^- increased at the vicinity of the zinc surface. Zn^{2+} ions from the $ZnCl_2$ reacted with OH^- ions and formed $Zn(OH)_4^{2}$ as building blocks and/or $Zn(OH)_2$ which is required for the formation of ZnO structures.

In the case of specimen B, thermal energy leads to diffusion of Zn atoms through the Au layer when the Au/Zn substrate (Zn substrate pre-coated with thin layer of Au) is heated. This result agrees well with previous reports [12,13] and it is expected that during the annealing process the rate of diffusion of Zn atoms from the substrates and formation of Au–Zn alloy for specimen B is greater than for specimen A. Fig. 1 shows the schematic illustrations of An–ZnO growth process.

The XRD patterns of the post-annealed specimens A and B at 400 °C for 4 h in air are seen in Fig. 2. All the XRD patterns show well-defined diffraction peaks, which are indexed to hexagonal wurtzite ZnO structures (JCPDS card no. 79-2205). In addition, other peaks corresponding to Au–Zn alloy are observed ($AuZn_3$: JCPDS card no. 29-0652 and Au_3Zn: JCPDS card no. 12-0084). It is interesting to note that the post-annealed specimen B shows formation of an $AuZn_3$ phase with higher relative intensity.

Fig. 3 shows SEM micrographs of the as-synthesized and post-annealed specimen A. The surface morphology of specimen A as seen in Fig. 3(a) is characterized by a network of densely packed and randomly oriented hexagonal flakes and sheets despite being mostly perpendicular to the substrate surface. The formation of randomly oriented sheets on the surface of the substrate may be attributed to the growth mechanism. It may be speculated that the OH^- generation rate increased after applying the voltage, caused by an increase in the formation of ZnO particles. These ZnO particles do not find new nucleation sites and attach to the sheet structures. The range of diameters of the hexagons is 2–10 μm, with average thickness ~500 nm. The SEM image of the post-annealed specimen A (Fig. 3(b)) shows the formation of cauliflower type agglomerate arrays on the entire substrate surface. A careful

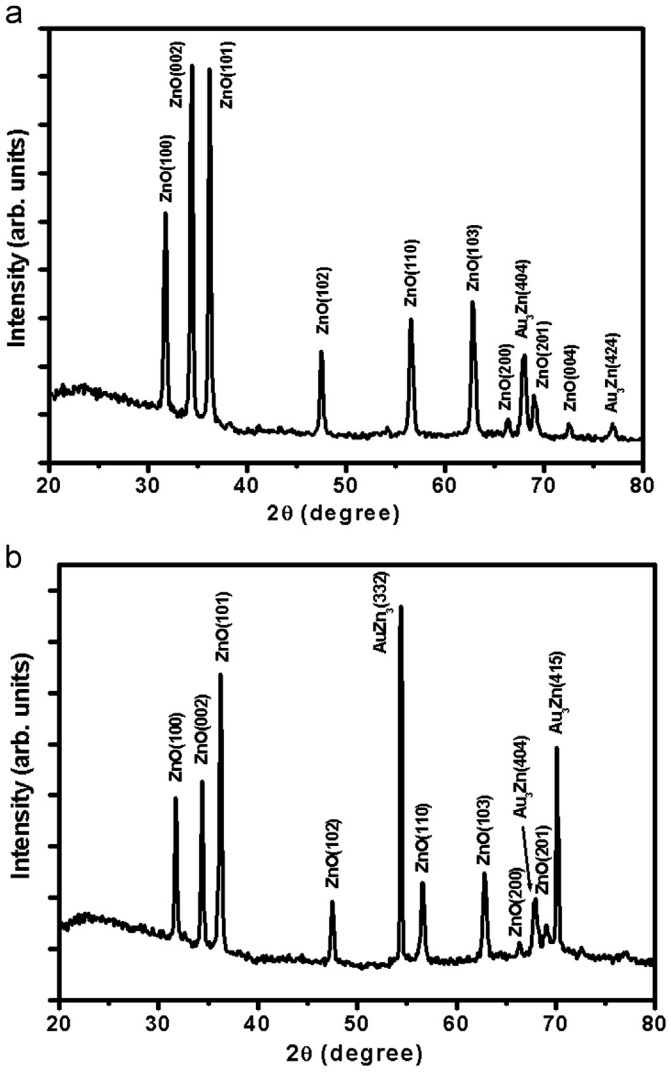

Fig. 2. XRD patterns of the Au–ZnO films synthesized using (a) electrochemical deposition (post-annealed specimen A) and (b) chemical solution deposition (post-annealed specimen B).

observation of the SEM (the inset of Fig. 3(b)) reveals the surface of each cauliflower consists of radial wires (diameter less than 120 nm) protruding outside the surface. As can be seen in Fig. 4, the SEM images of the post-annealed specimen B clearly show the formation of ZnO wires on the entire substrate surface. The ZnO wires have diameters in the range 70–400 nm and length of several microns. A closer inspection of the SEM micrographs reveals the ZnO wires, which are nearly aligned and tapered with diameter ~50 nm at the apex (the inset of Fig. 4).

From careful interpretation of the SEM micrograph, one may infer the growth mechanism of the post-annealed specimen A. It is expected that, this growth is similar to the growth mechanism of specimen B, which can explain the catalytic role of Au for growth of ZnO during the annealing process. Moreover the annealing process on specimen A includes two steps. The formation of cauliflower type agglomerate arrays and the growth of ZnO nanowire on the surface of the cauliflowers arising from electrodeposited zinc. The SEM

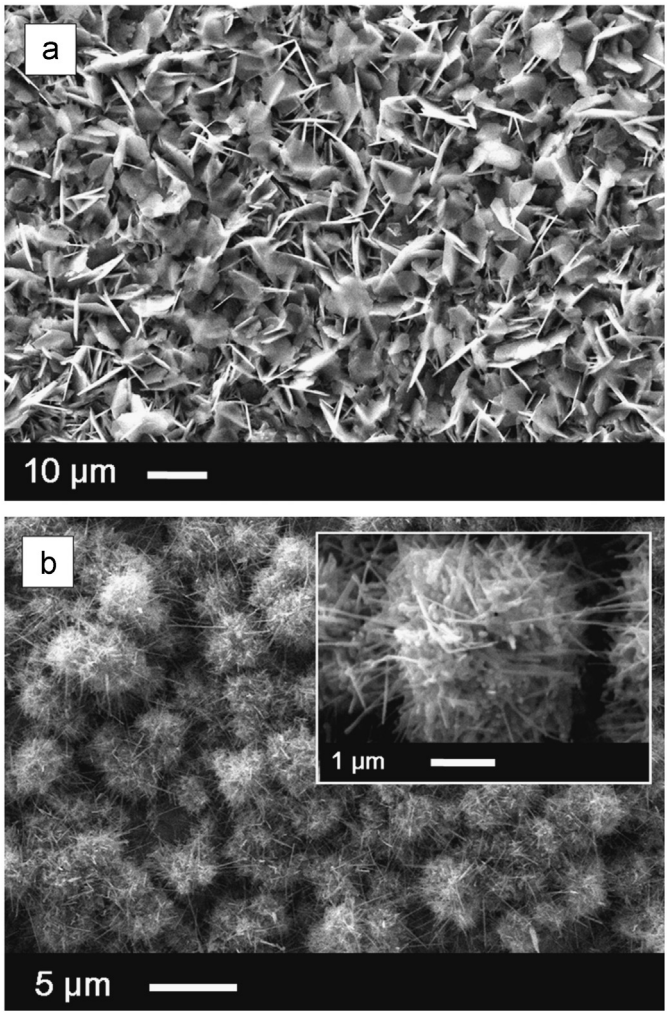

Fig. 3. SEM images of (a) as-synthesized and (b) post-annealed film prepared by electrochemical deposition (specimen A). The inset shows high magnification of the annealed specimen.

result shows that the diameters of ZnO nanowire synthesized via the annealing process of specimen A are smaller than those of specimen B. It can be concluded that the catalytic effect of Au when exposed is greater than when it is covered with a second layer such as the electrodeposited zinc in specimen A.

In the case of specimen A during the annealing process at 400 °C, gold can act as a catalyst capturing and condensing ZnO produced from the $Zn(OH)_2$ (s), while in the case of specimen B the diffusion of Zn atoms through the Au layer and reaction with O_2 (g) generates ZnO nanowire. Because of the different sources of Zn and O consumed in the formation of ZnO nanowire the compositional analysis (EDS) of the post-annealed specimens shows that the relative atomic percentage of O in specimen A is less than in specimen B. Moreover, the EDS results (not shown here for brevity) reveal the presence of Zn, O and Au only, indicating the chemical purity of the films.

Fig. 5 depicts the typical room temperature PL spectra of specimens A and B after annealing. The PL spectrum of ZnO has two emission bands. One is in the UV range (sharp band), which is associated with the near band edge transition of ZnO, specifically the recombination of free excitons. The other is in the visible range (broad band), which originates from electron-hole recombination at a deep level, presumably caused by oxygen and zinc vacancies, oxygen and zinc interstitials and surface states [14–17]. It is clear that the overall intensity of peaks in visible region corresponding to specimen A is higher than that of specimen B. This result indicates that more Au atoms might incorporate into the ZnO film during the annealing process, leading to the observed optical properties of the specimens. Furthermore, incorporation of Au atoms in the film can also affect the density of native point defects such as vacancies and interstitials. It is well known that native point defects generally play an important role in determining the electrical and optical properties of materials. This is due to the presence of localized levels/bands in the band gap of the materials. In addition, the EDS results show that the relative atomic percentage of oxygen is less in specimen A than in

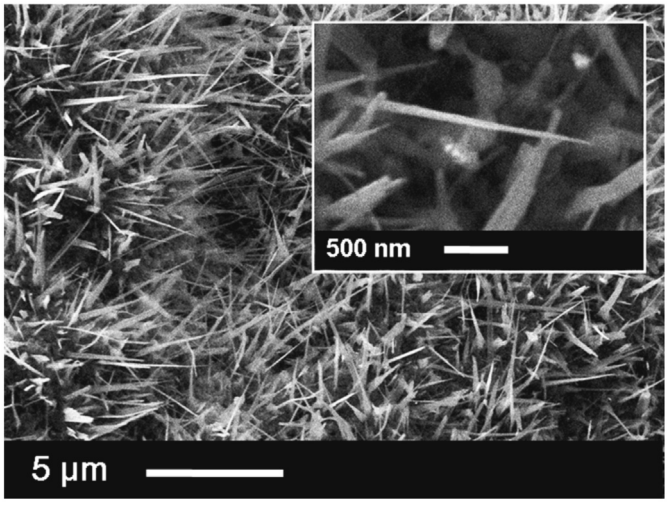

Fig. 4. SEM images of the Au–ZnO nanowire film synthesized using chemical solution deposition (post-annealed specimen B). The inset shows high magnification of the annealed specimen.

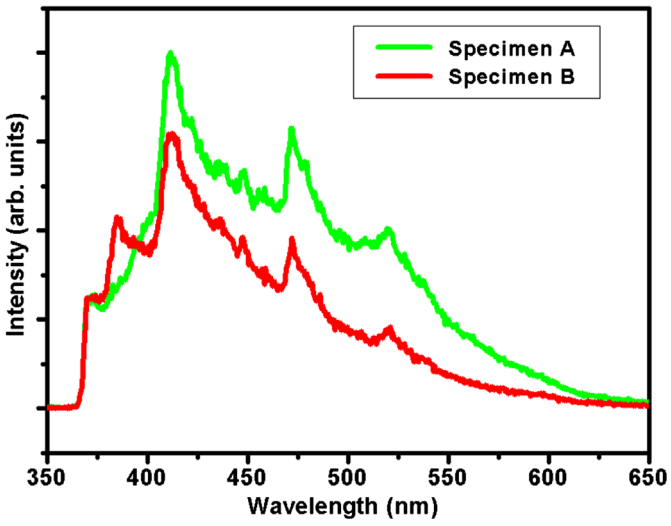

Fig. 5. PL spectra of the Au–ZnO nanowire films (post-annealed specimens A and B).

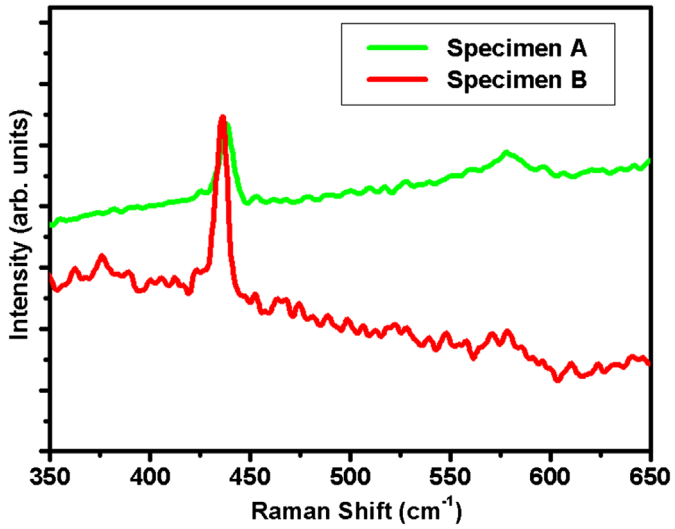

Fig. 6. Raman spectra of the Au–ZnO nanowire films (post-annealed specimens A and B).

specimen B, which suggests that the main reason for the higher peak intensity in the visible region is the presence of Au atoms and/or oxygen vacancies in the ZnO film.

Raman spectroscopy is an effective technique for determining the crystallinity of materials. According to group theory, single crystalline ZnO belongs to the C_{6V}^4 space group having two formula units per primitive cell, and eight sets of optical phonon modes at the Γ point of the Brillouin zone, classified as $A_1+E_1+2E_2$ modes (Raman active), $2B_1$ modes (Raman silent) and A_1+E_1 modes (infrared active). The E_1 mode is a polar mode and is split into transverse optical (TO), and longitudinal optical (LO) branches. Fig. 6 shows Raman spectra of specimens A and B after annealing. As shown in Fig. 6, the Raman spectra of both specimens show a sharp, strong, dominant peak at 437 cm^{-1} corresponding to the E_2 (high) mode of the Raman active mode, a characteristic peak for the wurtzite hexagonal phase of ZnO. A peak at 579 cm^{-1} corresponding to E_1 (LO) is present in both specimens. The E_1 (LO) mode is associated with impurities and formation of defects such as oxygen vacancies. The ratio of E_2 (high)/E_1 (LO) is the best way to compare crystalline quality of both specimens. This ratio is greater for specimen B than specimen A. Therefore, specimen B has higher crystallinity than specimen A. This result is in good agreement with the PL results.

4. Conclusions

Au–ZnO nanowire films have been fabricated by two separate chemical routes on zinc foil. The XRD patterns showed the presence of ZnO structure along with mixed phases of ZnO and Au. SEM images revealed the formation of nanowires with different morphology due to the catalytic action of Au during the annealing process. The PL studies demonstrated different concentrations of defects on the films. The Raman results indicated that Au–ZnO nanowire film prepared by the chemical bath deposition route had better crystalline quality than the electrodeposition method. This could be attributed to a decrease in oxygen vacancies and/or incorporation of Au on the ZnO nanowire film.

Acknowledgments

This work was supported by the Islamic Azad University, Ahwaz Branch, Ahwaz, Iran. F. Jamali-Sheini and R. Yousefi gratefully acknowledge the Islamic Azad University, Ahwaz and Masjed-Soleiman Branches, respectively, for their financial support in this research work.

References

[1] Ü. Özgür, I. Alivov, C. Liu, A. Teke, M.A. Reshchikov, S. Doğan, V. Avrutin, S.-J. Cho, H. Morkoç, A comprehensive review of ZnO materials and devices, Journal of Applied Physics 98 (2005) 041301–041404.
[2] F. Jamali-Sheini, Chemical solution deposition of ZnO nanostructure films: morphology and substrate angle dependency, Ceramics International 38 (2012) 3649–3657.
[3] Q. Ahsanulhaq, J.H. Kim, J.S. Lee, Y.B. Hahn, Electrical and gas sensing properties of ZnO nanorod arrays directly grown on a four-probe electrode system, Electrochemistry Communications 12 (2010) 475–478.
[4] H. Yu, Z. Zhang, M. Han, X. Hao, F. Zhu, A general low-temperature route for large-scale fabrication of highly oriented ZnO nanorod/nanotube arrays, Journal of the American Chemical Society 127 (2005) 2378–2379.
[5] Q. Ahsanulhaq, S.H. Kim, Y.B. Hahn, A templateless surfactant-free seedless aqueous route to single-crystalline ZnO nanowires synthesis, Journal of Physics and Chemistry of Solids 70 (2009) 627–631.
[6] F. Jamali-Sheini, R. Yousefi, Electrochemical synthesis and surface characterization of hexagonal Cu–ZnO nano-funnel tube films, Ceramics International 39 (2013) 3715–3720.
[7] Z.W. Pan, Z.R. Dai, Z.L. Wang, Nanobelts of semiconducting oxides, Science 291 (2001) 1947–1949.
[8] X.Y. Kong, Z.L. Wang, Spontaneous polarization-induced nanohelixes, nanosprings, and nanorings of piezoelectric nanobelts, Nano Letters 3 (2003) 1625–1631.
[9] N. Hongsith, C. Viriyaworasakul, P. Mangkorntong, N. Mangkorntong, S. Choopun, Ethanol sensor based on ZnO and Au-doped ZnO nanowires, Ceramics International 34 (2008) 823–826.
[10] S.J. Chang, T.J. Hsueh, I.C. Chen, B.R. Huang, Highly sensitive ZnO nanowire CO sensors with the adsorption of Au nanoparticles, Nanotechnology 19 (2008) 175502–175507.
[11] T. Chen, G.Z. Xing, Z. Zhang, H.Y. Chen, T. Wu, Tailoring the photoluminescence of ZnO nanowires using Au nanoparticles, Nanotechnology 19 (2008) 435711–435715.
[12] F. Jamali Sheini, D.S. Joag, M.A. More, J. Singh, O.N. Srivasatva, Low temperature growth of aligned ZnO nanowires and their application as field emission cathodes, Materials Chemistry and Physics 120 (2010) 691–696.
[13] F. Jamali-Sheini, R. Yousefi, K.R. Patil, Surface characterization of Au–ZnO nanowire films, Ceramics International 38 (2012) 6665–6670.
[14] Y. Kim, R. Seshadri, Optical properties of cation-substituted zinc oxide, Inorganic Chemistry 47 (2008) 8437–8443.
[15] V.A.L. Roy, A.B. Djurisic, W.K. Chan, J. Gao, H.F. Lui, C. Surya, Luminescent and structural properties of ZnO nanorods prepared under different conditions, Applied Physics Letters 83 (2003) 141–143.
[16] H. Shalish, V. Temkin, Narayanamurti, Size-dependent surface luminescence in ZnO nanowires, Physical Review B 69 (2004) 245401–245404.
[17] Q. Ahsanulhaq, J.H. Kim, N.K. Reddy, Y.B. Hahn, Growth mechanism and characterization of rose-like microspheres and hexagonal microdisks of ZnO grown by surfactant-free solution method, Journal of Industrial and Engineering Chemistry 14 (2008) 578–583.